Physics

Physics Research Publications

Purdue University *Year* 2011

Effect of oxygen plasma etching on graphene studied using Raman spectroscopy and electronic transport measurements

I. Childres L. A. Jauregui

J. F. Tian Y. P. Chen

This paper is posted at Purdue e-Pubs.
http://docs.lib.purdue.edu/physics_articles/1216

IOPscience iopscience.iop.org

Home Search Collections Journals About Contact us My IOPscience

Effect of oxygen plasma etching on graphene studied using Raman spectroscopy and electronic transport measurements

This article has been downloaded from IOPscience. Please scroll down to see the full text article.

2011 New J. Phys. 13 025008

(http://iopscience.iop.org/1367-2630/13/2/025008)

View the table of contents for this issue, or go to the journal homepage for more

Download details:
IP Address: 128.211.161.17
The article was downloaded on 21/04/2011 at 18:10

Please note that terms and conditions apply.

New Journal of Physics
The open-access journal for physics

Effect of oxygen plasma etching on graphene studied using Raman spectroscopy and electronic transport measurements

Isaac Childres[1,2], **Luis A Jauregui**[2,3], **Jifa Tian**[1,2] **and Yong P Chen**[1,2,3,4]

[1] Department of Physics, Purdue University, West Lafayette, IN 47907, USA
[2] Birck Nanotechnology Center, Purdue University, West Lafayette, IN 47907, USA
[3] School of Electrical and Computer Engineering, Purdue University, West Lafayette, IN 47907, USA
E-mail: yongchen@purdue.edu

New Journal of Physics **13** (2011) 025008 (12pp)
Received 29 October 2010
Published 10 February 2011
Online at http://www.njp.org/
doi:10.1088/1367-2630/13/2/025008

Abstract. In this paper, we report a study of graphene and graphene field effect devices after their exposure to a series of short pulses of oxygen plasma. Our data from Raman spectroscopy, back-gated field-effect and magnetotransport measurements are presented. The intensity ratio between Raman 'D' and 'G' peaks, I_D/I_G (commonly used to characterize disorder in graphene), is observed to initially increase almost *linearly* with the number (N_e) of plasma-etching pulses, but later decreases at higher N_e values. We also discuss the implications of our data for extracting graphene crystalline domain sizes from I_D/I_G. At the highest N_e value measured, the '2D' peak is found to be nearly suppressed while the 'D' peak is still prominent. Electronic transport measurements in plasma-etched graphene show an up-shifting of the Dirac point, indicating hole doping. We also characterize mobility, quantum Hall states, weak localization and various scattering lengths in a moderately etched sample. Our findings are valuable for understanding the effects of plasma etching on graphene and the physics of disordered graphene through artificially generated defects.

[4] Author to whom any correspondence should be addressed.

© IOP Publishing Ltd and Deutsche Physikalische Gesellschaft

Contents

1. Introduction 2
2. Experimental procedure 2
3. Results and analysis 3
4. Discussion 8
5. Summary 10

Acknowledgments 10

References 11

1. Introduction

Graphene has received much attention recently from the scientific community because of its distinct properties and potential in nanoelectronic applications. Many studies have reported on graphene's very high electrical conductivity at room temperature [1, 2] and its potential use in next-generation transistors [3], nanosensors [4], transparent electrodes [5] and many other applications.

Plasma etching is a common tool used to pattern graphene nanostructures, such as Hall bars [2] and nanoribbons [6]. In addition, plasma etching is used to study how graphene's properties are affected by etching-induced disorder [7]–[11]. Other techniques that have been used to create artificial defects in graphene include ozone exposure [12], high-temperature oxidation [13] and energetic irradiation by positive ions [14]–[20], protons [21] and electrons [22]–[27].

Previous reports have characterized oxygen plasma's effect on graphene's field effect conductivity [7, 8], Raman spectra [7, 8, 10], surface morphology as measured by atomic force microscopy (AFM) [7] and other properties [9, 10]. However, many aspects of the disorder generated by plasma etching in graphene remain to be better understood. For example, the initial stage of the disorder generation as reflected in Raman spectra (the so-called 'graphite to nanocrystalline graphite' stage [28]) has not been fully characterized because of the corresponding narrow window for the level of oxygen plasma exposure. The magnetotransport and carrier localization in plasma-etched graphene have also not been studied previously, to the best of our knowledge.

Here, we present a study of graphene exposed to various levels of oxygen plasma etching, with a focus on its properties as characterized by Raman, field-effect and magnetotransport measurements (including the quantum Hall effect and weak localization).

2. Experimental procedure

Our graphene samples are fabricated by micromechanical exfoliation [1] of highly ordered pyrolytic graphite (HOPG, 'ZYA' grade, Momentive Performance Materials) onto a p-doped Si wafer with 300 nm of SiO_2. Single-layer graphene flakes, typically about 100 μm^2 in size, are identified using color contrast with an optical microscope [29] and then confirmed using Raman spectroscopy (using a 532 nm excitation laser) [30]. Graphene field-effect devices are

Figure 1. The Plasma-Preen II-382 system operating at 100 W. Samples are placed under a Bell jar inside the modified microwave, where a controlled flow of oxygen is pumped through the jar and excited by microwave radiation.

fabricated using electron-beam lithography. The electrical contacts (5 nm-thick chromium and 35 nm-thick gold) are fabricated by electron-beam evaporation.

Our graphene devices are exposed cumulatively to short pulses (approximately 1/2 second) of oxygen plasma in a microwave plasma system (Plasma-Preen II-382, figure 1) operating at 100 W. A constant flow of O_2 is pumped through the sample space, and the gas is excited by microwave (manually pulsed on and off). The microwave generates an ionized oxygen plasma, which has an etching effect on graphene and thus creates defects (indeed etched holes can be observed by AFM, as was previously reported [7]). The microwave-excited plasma pulses are applied to the samples cumulatively, and field-effect and Raman measurements are carried out as soon as possible (~5 min) in ambient atmosphere and temperature after each pulse. The magnetotransport data are taken using a ^{3}He superconducting magnet probe several days after plasma exposure.

3. Results and analysis

Figure 2(a) shows representative Raman spectra for a single-layer graphene device (sample '1') taken after multiple cumulative exposures to oxygen plasma-etching pulses. Of particular interest is the disorder-induced characteristic Raman 'D' peak (~1350 cm^{-1}) [28] (other disorder-related peaks, such as the 'D'' (~1620 cm^{-1}) [28] and another peak ~2940 cm^{-1}, close to previously observed second-order features such as 'D + D'' [10] or 'D + G' [31], are also observed, but are relatively weak in intensity and we do not focus on them in this work). The 'D' peak initially rises with increasing exposure. After 14 pulses, the 'D' peak has ~4 times the amplitude of the graphene's 'G' peak (~1580 cm^{-1}), but with additional exposure the 'D' peak begins to attenuate along with the 'G' and '2D' (~2690 cm^{-1}) peaks (both of which begin to attenuate since the first exposure). After 23 pulses, the 'D' peak (while still significant) decreases to ~2 times the amplitude of the 'G' peak, and the '2D' peak is almost completely suppressed. Figure 2(b) shows the progression of the peak intensity ratios (I_D/I_G and I_{2D}/I_G) as functions of the number (N_e) of plasma-etching pulses. The dependence of the ratio of the intensities of the 'D' and 'G' peaks, I_D/I_G, on N_e shows two different behaviors in the regimes

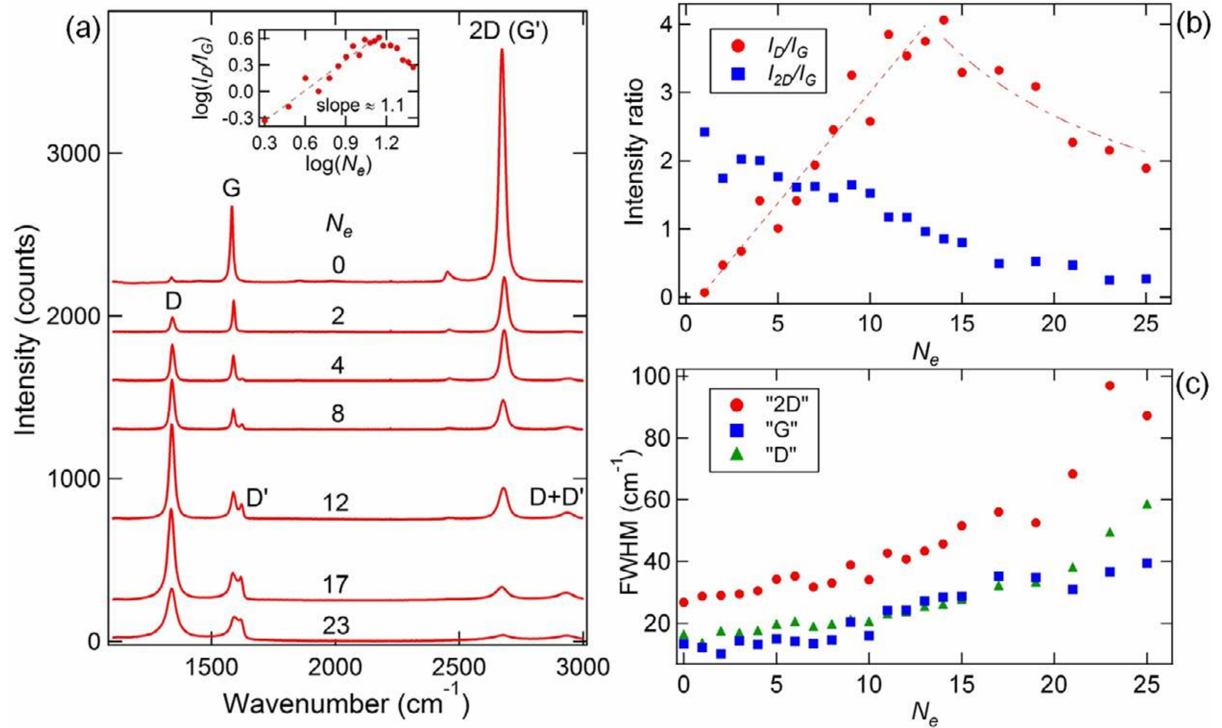

Figure 2. (a) Raman spectra of single-layer graphene sample '1' after various numbers of accumulated oxygen plasma pulses, N_e. The spectra are offset vertically for clarity. (b) Ratios of Raman peak intensities, I_D/I_G and I_{2D}/I_G, plotted versus N_e. The dashed line is a fit for $I_D/I_G = C \times L_e^{-2}$ (low-defect-density regime), and the dot-dashed line is a fit for $I_D/I_G = C \times L_e^2$ (high-defect-density regime), where $Le \propto 1/\sqrt{N_e}$. The inset of panel (a) shows $\log(I_D/I_G)$ against $\log(N_e)$. (c) The full-width at half-maximum of the '2D', 'G' and 'D' peaks plotted as functions of N_e.

of 'low' ($N_e < \sim 14$) and 'high' ($N_e > \sim 14$) defect densities (referred to as 'nanocrystalline graphite' and 'mainly sp^2 amorphous carbon' phases, respectively, in [28]). I_D/I_G begins at ~ 0 before the plasma exposure (the small 'D' peak is likely due to the device fabrication process), increases with increasing N_e in the low-defect-density regime to ~ 4 after 14 plasma exposures and then decreases with further increasing N_e in the high-defect-density regime to ~ 1.9 for $N_e = 25$. This non-monotonic behavior of I_D/I_G was also observed in recent electron-beam irradiation studies [22, 24]. On the other hand, the ratio of the intensities of the '2D' and 'G' peaks, I_{2D}/I_G, continuously decreases with increasing N_e from ~ 3 for $N_e = 0$ down to ~ 0.3 for $N_e = 25$. In figure 2(b), the data in the low-defect-density regime are fitted to

$$\frac{I_D}{I_G} = C \times N_e \quad \text{(dashed line)}, \tag{1}$$

and those in the high-defect-density regime are fitted to

$$\frac{I_D}{I_G} = \frac{C}{N_e} \quad \text{(dot-dashed line)}. \tag{2}$$

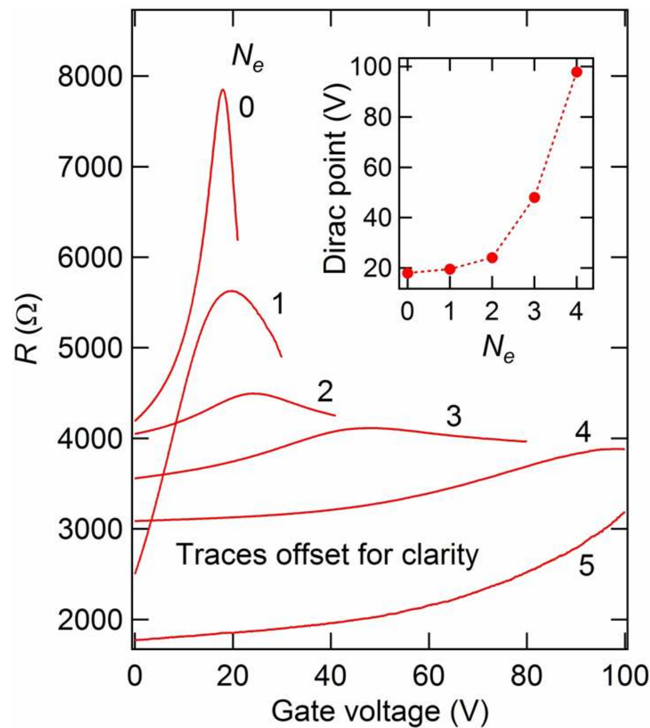

Figure 3. Measured resistance as a function of back-gate voltage of single-layer graphene sample '2' after various numbers of accumulated oxygen plasma pulses, N_e. The resistance values for different measurements are not directly comparable to each other because the measurement with $N_e = 0$ is four-terminal, the measurement with $N_e = 1$ is two-terminal and all others are three-terminal. The traces are offset vertically for clarity. The inset shows the CNP as a function of N_e.

The inset of figure 2(a) shows $\log(I_D/I_G)$ versus $\log(N_e)$. A line fit of the data in the low-defect-density regime gives a slope of $\sim$1.1, confirming the approximate linear relationship between I_D/I_G and N_e in that regime, as found in equation (1).

Figure 2(c) shows the full-width of the '2D', 'G' and 'D' peaks as functions of N_e. The peaks widen with increasing N_e, especially at higher exposures.

Figure 3 shows the measured field-effect resistance of another typical graphene device (sample '2'). The back-gate-dependent resistance is shown for various amounts of exposure up to a dosage where the charge-neutral 'Dirac' point (CNP) is no longer measurable within the gate voltage range used in our experiment. The inset of figure 3 shows the CNP as a function of N_e. The CNP voltage shifts to the positive direction with increasing plasma exposure, starting at 18 V before exposure and increasing to $\sim$100 V after four pulses. This $\sim$80 V of positive shift in the gate voltage corresponds to an increase in carrier concentration (n) by $\sim 6 \times 10^{12}$ cm^2.

A magnetotransport study is performed for a graphene field-effect device (sample '3') exposed to two oxygen plasma pulses. Prior to magnetotransport measurements, sample '3' is characterized by (four-terminal) field-effect conductivity measurements and Raman spectroscopy before and after exposure, and the results are shown in figures 4(a) and (b),

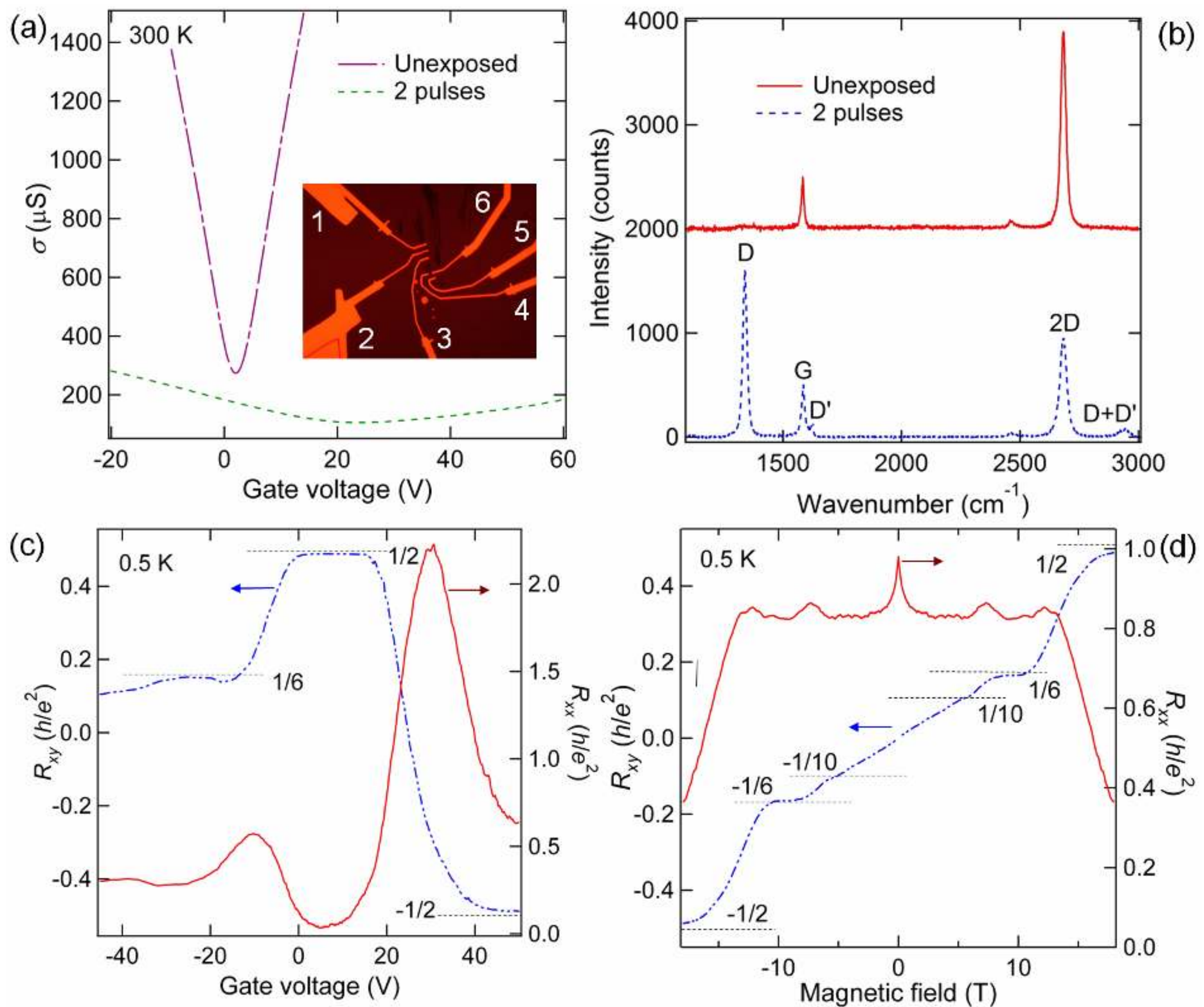

Figure 4. (a) Conductivity as a function of back-gate voltage measured in single-layer graphene sample '3' before and after two-oxygen plasma pulses. The inset of panel (a) is an optical image of sample '3'. For all electrical measurements, the current was supplied from lead 1 to lead 5, with R_{xx} measured from 3 to 4 and R_{xy} from 6 to 4. (b) Raman spectra of sample '3' taken before and after plasma exposure. The laser excitation wavelength is $\lambda = 532$ nm. The spectra are offset vertically for clarity. (c) Measured resistance as a function of back-gate voltage of post-exposure sample '3' at 18 T and 0.5 K. (d) Measured resistance as a function of magnetic field with no applied gate voltage under otherwise similar conditions to those in (c). The dashed lines in (c) and (d) indicate the locations of the expected quantum Hall plateaus in R_{xy} for filling factors 2, 6 and 10.

respectively. The CNP shifts from 2 V before exposure to 18 V after exposure, with the minimum conductivity (σ_{min}, taken as the conductivity at the CNP) decreasing from $\sim$275 to $\sim$100 μS. We can extract the field-effect mobility (μ_{FET}) by examining the slope of the field-effect curve, conductivity (σ) versus back-gate voltage (V_{g}), where V_{g} is sufficiently far away

from the CNP and the curve is in the linear regime, using [32]

$$\mu_{\mathrm{FET}} = \frac{t}{\varepsilon} \times \frac{\mathrm{d}\sigma}{\mathrm{d}V_{\mathrm{g}}}, \tag{3}$$

where $t = 300\,\mathrm{nm}$ is the thickness of the SiO_2 and $\varepsilon = 3.9 \times \varepsilon_0 = 3.45 \times 10^{-11}\,\mathrm{F\,m^{-1}}$ is the permittivity of the SiO_2. This gives room-temperature $\mu_{\mathrm{FET}} \approx 400\,\mathrm{cm^2\,V^{-1}\,s^{-1}}$ after exposure, compared to $\mu_{\mathrm{FET}} \approx 9800\,\mathrm{cm^2\,V^{-1}\,s^{-1}}$ before exposure.

The Raman spectra measured from sample '3' show the emergence of the characteristic 'D' peak after exposure, with $I_{\mathrm{D}}/I_{\mathrm{G}} \approx 3$.

Figure 4(c) shows the longitudinal resistance (four-terminal measurements), R_{xx}, and the Hall resistance, R_{xy}, versus V_{g} measured at a magnetic field of $B = 18\,\mathrm{T}$ (perpendicular to the graphene) and a temperature of $T = 0.5\,\mathrm{K}$ for sample '3'. R_{xy} plateaus at $\pm h/2e^2$ and $h/6e^2$, where h is the Planck constant and e is the electron charge. The plateaus can also be seen at filling factors $\nu = \pm 2$, ± 6 and ± 10 in the magnetic field sweep at 0.5 K with 0 V on the back gate, figure 4(d), where ν is defined by [1]

$$\nu = \frac{nh}{eB}. \tag{4}$$

The quantized Hall plateaus correspond to

$$R_{xy}^{-1} = \pm \frac{\nu e^2}{h} \quad \text{with } \nu = 4\left(N + \frac{1}{2}\right). \tag{5}$$

We can also calculate mobility from the Hall effect measured in figure 4(d) using [32]

$$\mu_{\mathrm{HALL}} = \frac{R_{\mathrm{H}}}{\rho_{xx}(B=0)}, \quad \text{where } R_{\mathrm{H}} = \frac{\mathrm{d}R_{xy}}{\mathrm{d}B} \text{ at low } B. \tag{6}$$

This yields a post-exposure Hall mobility of $\sim 600\,\mathrm{cm^2\,V^{-1}\,s^{-1}}$. We also note a pronounced peak in $R_{xx}(B=0)$. This peak is due to weak localization, which is typically suppressed in low-disorder single-layer graphene devices [33].

$R_{xx}(B)$ measurements in low B are also taken from sample '3' at various temperatures ranging from 0.5 to 60 K and $V_{\mathrm{g}} = 10\,\mathrm{V}$, shown in figure 5(a). These data characterize weak localization in the sample. Weak localization arises from the constructive interference between time-reversed multiple scattering trajectories of phase coherent carriers, leading to coherent back-scattering of carriers and increasing the electrical resistance. When a perpendicular magnetic field is introduced to break time-reversal symmetry or the temperature is raised to destroy phase coherence, this interference is suppressed. From the low magnetic field data, we can extract the phase coherence length, L_φ, as well as the intervalley and intravalley scattering lengths, L_i and L_*, respectively, using [34]–[36]

$$\Delta\sigma_{xx}(B) = \frac{e^2}{\pi h} \times \left[F\left(\frac{B}{B_\varphi}\right) - F\left(\frac{B}{B_\varphi + 2B_i}\right) - 2F\left(\frac{B}{B_\varphi + B_i + B_*}\right)\right]$$

$$\text{with } F(z) = \ln(z) + \Psi\left(\frac{1}{2} + \frac{1}{z}\right) \quad \text{and} \quad B_{\varphi,i,*} = \left(\frac{h}{8\pi e}\right) L_{\varphi,i,*}^{-2},$$

$$\text{where } \Delta\sigma_{xx}(B) = [\sigma_{xx}(B) - \sigma_{xx}(B=0)] - [\sigma_{xx}(B, T_{\mathrm{h}}) - \sigma_{xx}(B=0, T_{\mathrm{h}})]$$

$$\text{and} \quad \sigma_{xx}(B) = \frac{l}{w} \times \frac{1}{R_{xx}(B)}. \tag{7}$$

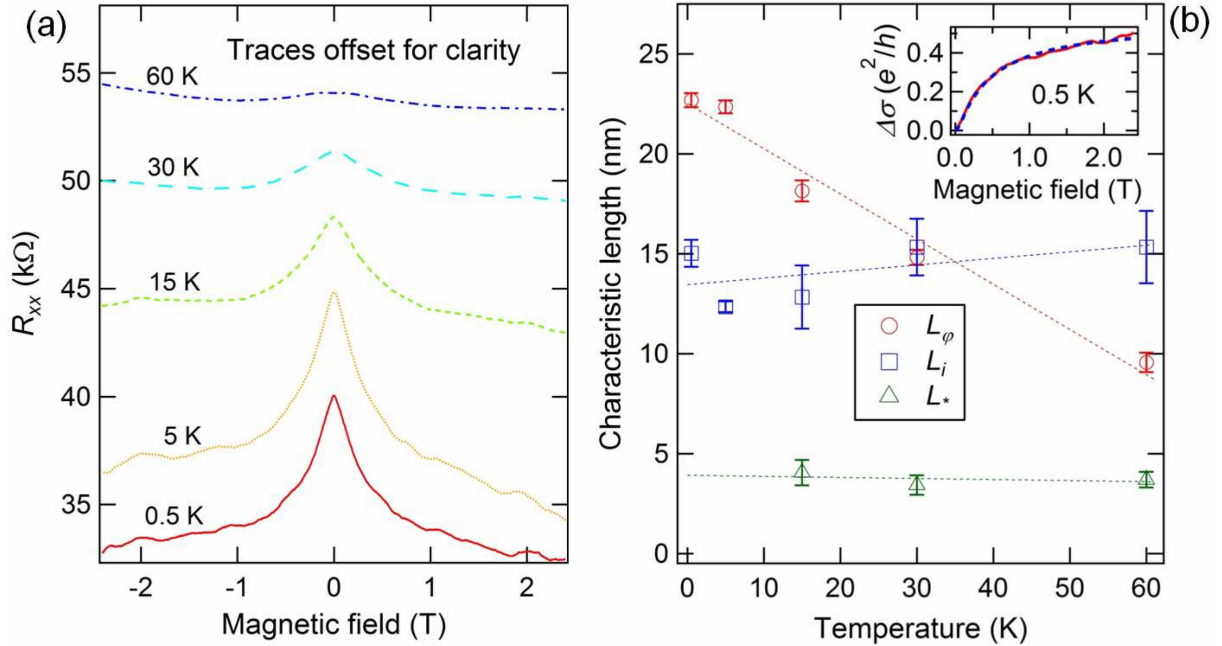

Figure 5. Temperature-dependent magnetoresistance (four-terminal measurements) showing weak localization in sample '3' after two pulses of oxygen plasma. (a) Magnetoresistance, $R_{xx}(B)$, measured at various temperatures. The traces are offset vertically for clarity. (b) Extracted characteristic lengths from weak localization fittings as functions of temperature. The inset shows magnetic-field-dependent $\Delta\sigma$ (solid line) and the result of fitting (dashed line) using equation (4) to extract L_φ, L_i and L_*. $\Delta\sigma$ has been symmetrized between two opposite magnetic field directions.

The l and w denote the length and width of the graphene device, Ψ is the digamma function and $\sigma(B,T_\mathrm{h})$ represents the magnetoconductivity at a sufficiently high temperature (approximated using data at $T = 60\,\mathrm{K}$) for the weak localization feature to disappear. From the plots of these characteristic lengths as a function of temperature, seen in figure 5(b), we note that the elastic scattering lengths L_i and L_* are relatively T-insensitive, averaging $\sim$14 and $\sim$4 nm, respectively. Intravalley scattering is believed to be largely caused by charge impurity disorder, whereas intervalley scattering is caused by sharp lattice defects [34]–[36]. We also note that the inelastic scattering (phase-breaking) length L_φ decreases with increasing T (which reduces the phase coherence of electrons) from $\sim$23 nm at 0.5 K to $\sim$10 nm at 60 K. The temperature-dependent trends for L_φ, L_i and L_* are qualitatively consistent with previous reports [35, 36].

4. Discussion

The Raman spectrum taken before exposure indicates single-layer graphene with $I_{2\mathrm{D}}/I_\mathrm{G} > 2$ and a symmetric Lorentzian 2D peak [30]. The evolution of $I_\mathrm{D}/I_\mathrm{G}$ as a function of induced plasma disorder can be attributed to a gradual evolution from the sp^2-bonded carbon found in graphene into amorphous carbon with appreciable sp^3 bonding [28]. This evolution is classified

into two main regimes—a so-called ‘graphite to nanocrystalline graphite’ phase characterized by increasing I_D/I_G with increasing disorder (or ‘low-defect-density regime’) and a so-called ‘nanocrystalline graphite to mainly sp^2 amorphous carbon’ phase characterized by decreasing I_D/I_G with increasing disorder (or ‘high-defect-density’ regime) [28].

In the low-defect-density regime, an empirical formula known as the Tuinstra–Koenig relation [28, 37, 38] has been developed to extract the crystalline domain size L_d (which also characterizes the average separation between defects) for disordered graphite,

$$\frac{I_D}{I_G} = \frac{C(\lambda)}{L_d}, \quad \text{where } C(\lambda) = (2.4 \times 10^{-10}\,\text{nm}^{-3}) \times \lambda^4, \tag{8}$$

and λ is the Raman excitation wavelength (532 nm in our case). In the high-defect-density regime, it has been proposed that I_D/I_G versus L_d can be fitted to the equation [28, 38]

$$\frac{I_D}{I_G} = D(\lambda) \times L_d^2, \tag{9}$$

where the constant $D(\lambda)$ is obtained by imposing continuity between the two regimes.

Recent work [16], however, has suggested a new relationship between I_D/I_G and L_d for disordered graphene, in the low-defect-density regime as

$$\frac{I_D}{I_G} = \frac{C'(\lambda)}{L_d^2}. \tag{10}$$

This formula has been proposed as an approximation for a physical model considering the total area contributing to Raman scattering in the case of relatively isolated and dilute defects created by irradiation (versus 1D-like line defects separating crystallites) [16].

In our experiment, we assume the total exposure time to be proportional to the defect concentration, $1/L_d^2$; therefore $L_d \propto 1/\sqrt{N_e}$.

We find that our data agree with equation (9) in the high-defect-density regime (dot-dashed line fit in figure 2(b)). However, in the low-defect-density regime (dashed line fit in figure 2(b)), our data are better fitted to equation (10) than to equation (8). $C'(\lambda)$ is given as 102 nm^2 for $\lambda = 514$ nm [16]. Assuming comparable $C'(\lambda)$ for our slightly different λ (532 nm) in equation (10), we estimate that $L_d \approx 5$ nm at the peak of I_D/I_G ($\sim$4), a value similar to other reported values [16, 20].

The gradual decrease in the ‘2D’ peak is also consistent with previous work [7, 9, 13]. The decreasing I_{2D}/I_G versus N_e is probably due to a combination of the positive doping of the graphene and the defect-induced suppression of the lattice vibration mode corresponding to the 2D peak.

The field-effect measurements show a strong positive shift in the CNP after plasma etching, most likely caused by p-doping molecules from the ambient, e.g. water, attaching to the defects (e.g. edges of etched holes) [39][5]. If we use data in figure 2 as a guideline, four plasma pulses (which caused the CNP to up-shift by $\sim$80 V, indicating a carrier density increase of $\sim 6 \times 10^{12}$ cm^2) give $I_D/I_G \approx 1.4$, from which we extract (using equation (10)) $L_d \approx 9$ nm, which corresponds to an effective defect concentration of $\sim 8.4 \times 10^{11}$ cm^2. We therefore estimate an effective doping per defect of $\sim$7 holes on average. While the hole doping

[5] Our ascription for the majority of the up-shift in the CNP as due to weakly bonding p-doping adsorbates such as water is also consistent with our observation that pumping our exposed samples in vacuum gives a substantial reduction in the up-shift in CNP (i. e. bringing it down toward the pre-exposure value.)

is also expected to cause a small blue shift in the Raman 'G' peak position [40], this is not resolved due to the resolution of our Raman measurements.

The electrical transport measurements show that the oxygen plasma exposure significantly decreases the sample's $\sigma_{\min}$ (at the Dirac point) and mobility. Interestingly, even with this high level of disorder and low mobility (accompanied by pronounced weak localization), we still observe the half-integer quantum Hall effect in the form of well-developed plateaus in R_{xy}, corresponding to Landau level filling factors at 2, 6 and 10. We also note in figure 4(d) that although the quantum Hall plateaus in R_{xy} are reasonably well developed for $\nu = \pm 6$ and ± 10, the corresponding R_{xx} (which normally approaches 0 for quantum Hall effect states) still take substantial values ($>\sim 0.8\,\mathrm{h\,e^{-2}}$). Further studies are needed for a better understanding of this behavior and whether it could be related to, for example, a proposed 'dissipative' quantum Hall effect [41] or charge inhomogeneity (puddles) [39] in graphene.

A comparison of the measured Raman spectrum from sample '3' after exposure with the spectra in figure 2 shows that the sample is in the low-defect-density regime. For $I_D/I_G \approx 3$ (figure 4(b)), we can calculate that $L_d \approx 6\,\mathrm{nm}$ from equation (10). This is of a similar order of magnitude as L_i ($\sim$14 nm) and L_* ($\sim$4 nm) extracted from weak localization fitting. Although it is still difficult to pinpoint exactly what kinds of disorder in graphene give rise to these scattering lengths, it has been proposed that atomically sharp defects largely contribute to L_i, whereas larger-length-scale disorder, such as charged impurities, can contribute to L_* [12, 33]. Such disorder and their effects do not strongly depend on temperature [35], hence the relative insensitivity of L_i and L_* to T.

5. Summary

In summary, we have studied the disorder in graphene caused by oxygen plasma etching. Raman spectra show a characteristic progression of I_D/I_G with an increasing level of disorder, indicating an evolution from a graphene lattice to a more amorphous carbon phase in two distinct regimes, in which we can empirically extract defect length scales from I_D/I_G. The field effect in plasma-etched graphene shows a decrease in mobility and minimum conductivity, as well as a positive shift in the CNP voltage, indicating p-dopants attaching to the defect sites. Weak localization analysis reveals information about disorder-induced scattering, while well-developed quantum Hall plateaus are still observed in moderately etched samples. These results are valuable in understanding the effect of oxygen plasma etching on graphene as well as the nature of disorder in graphene.

Acknowledgments

This work was partially supported by the National Science Foundation (ECCS no. 0833689), Department of Homeland Security (no. 2009-DN-077-15 ARI036-02) and Defense Threat Reduction Agency (HDTRA1-09-1-0047). The donors of the American Chemical Society Petroleum Research Fund are acknowledged for partial support of this research. Part of this work was carried out at the National High Magnetic Field Laboratory, which is supported by NSF Cooperative Agreement No. DMR-0084173, by the State of Florida and DOE. YPC acknowledges support from the Miller Family Endowment and IBM. We thank Ken Smith and Andrew Haefner of Thermo Fisher Scientific for assistance in Raman measurements. We thank Ju-Hyun Park and Eric Palm for assistance with experiments.

References

[1] Geim A K and Novoselov K S 2007 *Nat. Mater.* **6** 183
[2] Berger C *et al* 2006 *Science* **312** 1191
[3] Schwierz F 2010 *Nat. Nanotechnol.* **5** 487
[4] Schedin F, Geim A K, Morozov S V, Hill E W, Blake P, Katsnelson M I and Novoselov K S 2007 *Nat. Mater.* **6** 652
[5] Bae S *et al* 2010 *Nat. Nanotechnol.* **5** 574
[6] Han M Y, Ozyilmaz B, Zhang Y B and Kim P 2007 *Phys. Rev. Lett.* **98** 206805
[7] Kim D C, Jeon D-Y, Chung H-J, Woo Y S, Shin J K and Seo S 2009 *Nanotechnology* **20** 375703
[8] Kim K, Park H J, Woo B-C, Kim K J, Kim G T and Yun W S 2008 *Nano Lett.* **8** 3092
[9] Shin Y J, Wang Y Y, Huang H, Kalon G, Thye A, Wee S, Shen Z, Bhatia C S and Yang H 2010 *Langmuir* **26** 3798
[10] Gokus T, Nair R R, Bonetti A, Boehmler M, Lombardo A, Novoselov K S, Geim A K, Ferrari A C and Hartschuh A 2009 *ACS Nano* **3** 3963
[11] Kim K-J, Choi J, Lee H, Jung M C, Shin H J, Kang T-H, Kim B and Kim S 2010 *J. Phys.: Condens. Matter* **22** 045005
[12] Moser J, Tao H, Roche S, Alzina F, Torres C M S and Bachtold A 2010 *Phys. Rev.* B **81** 205445
[13] Liu L, Ryu S, Yomasik M R, Stolyarova E, Jung N, Hybertsen M S, Steigerwald M L, Brus L E and Flynn G W 2008 *Nano Lett.* **8** 1965
[14] Giannazzo F, Sonde S, Raineri V and Rimini E 2009 *Appl. Phys. Lett.* **95** 263109
[15] Compagnini G, Giannazzo F, Sonde S, Raineri V and Rimini E 2009 *Carbon* **47** 3201
[16] Lucchese M M, Stavale F, Ferreira E H, Vilani C, Moutinho M V O, Capaz R B, Achete C A and Jorio A 2010 *Carbon* **48** 1592
[17] Tapaszto L, Dobrik G, Nemes-Incze P, Vertesy G, Lambii P and Biro L P 2008 *Phys. Rev.* B **78** 233407
[18] Chen J-H, Cullen W G, Jang C, Fuhrer M S and Williams E D 2009 *Phys. Rev. Lett.* **102** 236805
[19] Lopez J J, Greer F and Greer J R 2010 *J. Appl. Phys.* **107** 104326
[20] Tan C L, Tan Z B, Ma L, Qu F M, Yang F, Chen J, Liu G T, Yang H F, Yang C L and Lu L 2009 *Sci. China* G **52** 1293
[21] Arndt A, Spoddig D, Esquinazi P, Barzola-Quiquia J, Durari S and Butz T 2009 *Phys. Rev. B* **80** 195402
[22] Teweldebrhan D and Balandin A A 2009 *Appl. Phys. Lett.* **94** 013101
[23] Teweldebrhan D and Balandin A A 2009 *Appl. Phys. Lett.* **95** 246101
[24] Liu G, Teweldebrhan D and Balandin A 2010 *IEEE Trans. Nanotechnol.* doi:10.1109/TNANO.2010.2087391 arXiv:1012.5061v1
[25] Rao G, Mctaggart S, Lee J L and Geer R E 2009 *Mater. Res. Soc. Symp. Proc.* **1184** -HH03–07
[26] Xu M, Fujita D and Hanagata N 2010 *Nanotechnology* **21** 265705
[27] Childres I, Jauregui L A, Foxe M, Tian J, Jalilian R, Jovanovic I and Chen YP 2010 *Appl. Phys. Lett.* **97** 173109
[28] Ferrari A C 2007 *Solid State Commun.* **143** 47
[29] Blake P, Hill E W, Castro Neto A H, Novoselov K S, Jiang D, Yang R, Booth T J and Geim A K 2007 *Appl. Phys. Lett.* **91** 063124
[30] Ferrari A C, Meyer J C, Scardaci V, Casiraghi C, Lazzeri M, Mauri F, Piscanec S, Jiang D, Novoselov K S, Roth S and Geim A K 2006 *Phys. Rev. Lett.* **97** 187401
[31] Campos-Delgado J *et al* 2008 *Nano Lett.* **8** 2773
[32] Novoselov K S, Geim A K, Morozov S V, Jiang D, Zhang Y, Dubonos S V, Grigorieva I V and Firsov A A 2004 *Science* **306** 666
[33] Morozov S V, Novoselov K S, Katnelson M I, Schedin F, Ponomarenko L A, Jiang D and Geim A K 2006 *Phys. Rev. Lett.* **97** 016801
[34] McCann E, Kechedzhi K, Fal'ko V I, Suzuura H, Ando T and Altshuler B L 2006 *Phys. Rev. Lett.* **97** 146805

[35] Tikhonenko F V, Horsell D W, Gorbachev R V and Savchenko A K 2008 *Phys. Rev. Lett.* **100** 056802
[36] Mucciolo E R and Lewenkopf C H 2010 *J. Phys.: Condens. Matter* **22** 273201
[37] Tuinstra F and Koenig J L 1970 *J. Chem. Phys.* **53** 3
[38] Cancado L G, Takai K and Enoki T 2006 *Appl. Phys. Lett.* **88** 163106
[39] Jalilian R, Jauregui L A, Lopez G, Tian J, Roecker C, Yazdanpanah M M, Cohn R W, Jovanovic I and Chen Y P 2010 arXiv:1003.5404v1
[40] Das A *et al* 2008 *Nat. Nano.* **3** 210
[41] Abanin D A, Novoselov K S, Zeitler U, Lee P A, Geim A K and Levitov L S 2007 *Phys. Rev. Lett.* **98** 196806